

Supplementary Information for

**Fluorescence quantum yields of dye aggregates: A showcase example based on self-
assembled perylene bisimide dimers**

Franziska Fennel,^a Jana Gershberg,^b Matthias Stolte,^{a,b} and Frank Würthner^{a,b,*}

^a Center for Nanosystems Chemistry (CNC) & Bavarian Polymer Institute (BPI), Universität
Würzburg, Theodor-Boveri-Weg, 97074 Würzburg.

^b Institut für Organische Chemie, Universität Würzburg, Am Hubland, 97074 Würzburg,

E-mail: wuerthner@uni-wuerzburg.de

Table of contents

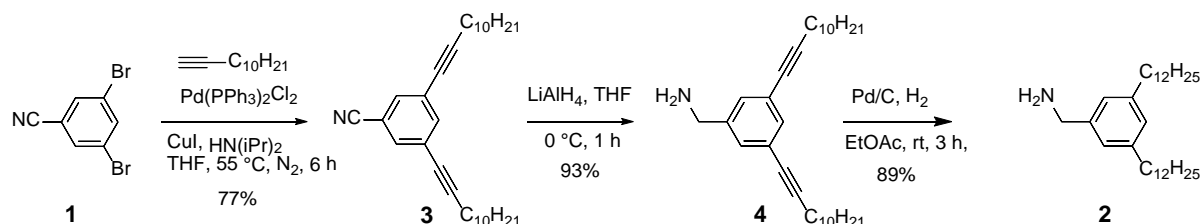
1. Materials and methods.....	3
2. Synthesis and characterization of PBI 2.....	4
3. ¹ H NMR and mass spectra of PBI 2	8
4. Aggregation of PBI 2	9
5. Determination of the fluorescence quantum yields of PBI 1 and PBI 2 monomers.....	13
6. Calibration of monochromators.....	13
7. Conditions for self-absorption free emission of PBIs	17
8. Excitation wavelength dependent emission of fluorescence standard PBI-ref 2 and PBI 2 in toluene	19
9. Scan of excitation wavelength for species averaged method	20
10. Determination of ratio of excited monomers from the aggregation study.....	21
11. Determination of aggregate quantum yield of PBI1 with species averaged method.....	22
12. Histogram of aggregate size for characteristic concentrations.....	23
13. Error discussion.....	24
14. References	25

1. Materials and methods

Solvent and reagents were purchased from commercial sources, unless otherwise stated, and purified and dried according to standard procedures.^[S1] Reactions were monitored by TLC on silica gel plates (Merck TLC silica gel 60 F254 aluminum sheets). Column chromatography was performed on silica gel (MerckSilica 60, particle size 0.04 – 0.063 mm). Gel permeation chromatography (GPC) was performed on a Shimadzu Recycling GPC system (LC-20AD prominence pump; SPDMA20A, prominence diode array detector) using three preparative columns (JAIGEL-1H, JAIGEL-2H und JAIGEL-2.5H) from Japan Analytical Industries Co., Ltd. and chloroform as eluent. NMR experiments were conducted on a Bruker Avance 400 or Bruker DMX 600 spectrometer with TMS or residual undeuterated solvent as internal standard. The chemical shifts are reported in ppm relative to TMS or residual undeuterated solvent as internal standard (δ scale). The apparent coupling constants J are given in Hertz (Hz). The following abbreviations are used to describe the signal fine structure: s = singlet, s_{br} = broad singlet, d = doublet, t = triplet, q = quartet, quint = quintet, dd = doublet of doublets, m = multiplet, and bm = broad multiplet. Melting point was measured on a polarization microscope BX41 of Olympus equipped with MGW Lauda RM6 cooling systems and is uncorrected. High-resolution electrospray ionization (ESI) mass spectra were measured on a MicroTOF Focus instrument (Bruker Daltronik GmbH).

2. Synthesis and characterization of PBI 2

Compound **3** was synthesized by a Sonogashira cross-coupling reaction of the commercially available 3,5-dibromobenzonitrile (**1**) and 1-dodecyne (**2**) in 77 % yield. The reduction of the nitrile group in **3** by LAH afforded the compound **4** in 93 % yield. Afterwards, the second reduction by Pd/C and H₂ gave the desired amine **2** with the yield of 89 % (Scheme S1).



Scheme S1: Synthetic route to the benzylamine **2**.

3,5-Di(dodec-1-yn-1-yl)benzonitril (**3**)

1-Dodecyne (960 mg, 5.76 mmol, 3 eq.) was added to a degassed suspension of 3,5-dibromobenzonitrile (500 mg, 1.92 mmol, 1 eq.), copper(I) iodide (10.9 mg, 57.6 μmol, 0.03 eq.) and bis(triphenylphosphine)palladium(II) dichloride (40.4 mg, 57.6 μmol, 0.03 eq.) in a mixture of 15 ml diisopropylamine and 20 ml THF. After further degassing, the reaction mixture was stirred for 19 h at 55 °C followed by filtration through a pad of celite. The solvent was removed under reduced pressure and the crude product was purified by silica gel column chromatography (eluent: dichloromethane:hexane 4:6) to yield **3** as a brown viscous oil.

Yield: 640 mg (1.48 mmol, 77 %). MW (C₃₁H₄₅N) 431.71 g/mol; ¹H NMR (400 MHz, CDCl₃): δ = 7.57 (t, ⁴J = 1.5 Hz, 1H), 7.51 (d, ⁴J = 1.5 Hz, 2H), 2.38 (t, ³J = 7.6 Hz, 4H), 1.62–1.54 (m, 4H), 1.46–1.38 (m, 4H), 1.33–1.25 (m, 24H), 0.88 (t, ⁴J = 7.0 Hz, 6H); ¹³C NMR (100 MHz, CDCl₃): δ = 138.6, 133.5, 125.9, 117.9, 112.9, 93.9, 78.2, 32.0, 29.7, 29.6, 29.5, 29.3, 29.0, 28.6, 22.8, 19.5, 14.3; HRMS (ESI pos.; MeOH), calculated for ([M+H]⁺): 432.362, found *m/z*

= 432.362; elemental analysis calculated (%) for C₃₁H₄₅N: C 86.25, H 10.51, N 3.24; found: C 86.14, H 10.23, N 3.40.

3,5-Di(dodec-1-yn-yl)phenyl)benzylamine (4)

Under an atmosphere of nitrogen, a solution of 3,5-di(dodec-1-yn-1-yl)benzotrile (3) (350 mg, 810 μmol, 1 eq.) in 4 ml dry diethyl ether was added to a suspension of lithium aluminum hydride (61.2 mg, 1.62 mmol, 2 eq.) in 3 ml dry diethyl ether at 0°C within 5 minutes. After stirring the suspension for 1 h at room temperature, the reaction was quenched by the addition of water and extracted three times with each 50 ml diethyl ether. The combined organic layers were dried over Na₂SO₄ and the solvent was removed under reduced pressure to yield 4 as a yellow viscous oil.

Yield: 340 mg (780 μmol, 93 %). MW (C₃₁H₄₉N) 435.74 g/mol; ¹H NMR (400 MHz, CDCl₃): δ = 7.30 (t, ⁴J = 1.4 Hz, 1H), 7.23 (d, ⁴J = 1.5 Hz, 2H), 3.78 (s, 2H), 2.37 (t, ³J = 7.0, 4H), 1.61-1.54 (m, 4H), 1.46-1.39 (m, 4H), 1.33-1.27 (m, 26H), 0.87 (t, ³J = 7.0 Hz, 6H); ¹³C NMR (100 MHz, CDCl₃): δ = 143.6, 133.1, 129.4, 124.5, 90.9, 80.1, 46.1, 32.1, 29.7, 29.6, 29.5, 29.3, 29.1, 28.9, 22.8, 19.5, 14.3; HRMS (ESI pos.; acetonitrile/CHCl₃), calculated for ([M+H]⁺): 436.393, found *m/z* = 436.393; elemental analysis calculated (%) for C₃₁H₄₉N: C 85.45, H 11.34, N 3.21; found: C 85.24, H 11.12, N 3.22

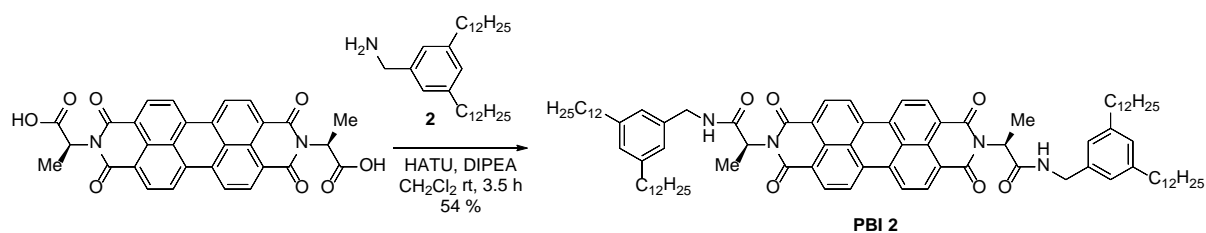
3,5-Didodecylbenzylamine (2)

Pd/C (100 mg with 10 wt. % loading) was added to a solution of 3,5-di(dodec-1-yn-yl)phenyl)benzylamine (4) (250 mg, 570 μmol) in 20 ml ethyl acetate. After stirring for 3 h at room temperature under an atmosphere of hydrogen (1013 mbar), the suspension was filtered

through a pad of celite and the solvent was removed under reduced pressure to yield **2** as a colorless solid

Yield: 227 mg (510 μ mol, 89 %). MW (C₃₁H₅₇N) 443.80 g/mol; m.p.: 57-60°C; ¹H NMR (400 MHz, CDCl₃): δ = 6.80 (s, 2H), 6.79 (s, 1H), 2.53 (t, ³J = 7.7 Hz, 4H), 2.29 (s, 2H), 1.63–1.54 (m, 4H), 1.35–1.23 (m, 38H), 0.88 (t, ³J = 6.6 Hz, 6H); ¹³C NMR (100 MHz, CDCl₃): δ = 143.0, 137.7, 126.6, 125.8, 36.1, 32.1, 31.8, 30.0, 29.9, 29.8, 29.77, 29.70, 29.6, 29.5, 22.8, 21.5, 14.3; HRMS (ESI pos.; acetonitrile/CHCl₃), calculated for ([M+H]⁺): 444.456, found *m/z* = 444.457.

***N,N'*-(*L*-alanyl(3,5-bis(dodecyl)benzyl))perylene-3,4:9,10-tetracarboxylic acid bisimide (PBI 2)**



Scheme S2: Synthetic route to perylene bisimide PBI 2.

A suspension of the *L*-alanine-functionalized PBI *N,N'*-di((*S*)-1-carboxylethyl)-3,4:9,10-perylenetetracarboxylic acid bisimide^[S2] (116 mg, 0.210 mmol, 1 eq), 3,5-didodecylbenzylamine **2** (289 mg, 0.651 mmol, 3 eq.), *O*-(7-azabenzotriazol-1-yl)-*N,N,N',N'*-tetra-methyluronium hexafluorophosphate (HATU) (200 mg, 0.526 mmol, 2.4 eq.) and *N,N*-diisopropylethylamine (DIPEA) (1.6 ml) was stirred in anhydrous dichloromethane (20 ml) at room temperature for 3.5 h. After removal of the solvent in vacuo, the crude product was purified by column chromatography (SiO₂, CH₂Cl₂/MeOH/NEt₃, v/v/v = 98:1.5:0.5).

Yield: 163 mg (0.117 mmol, 54 %) of a red solid; MW ($C_{92}H_{128}N_4O_6$) 1386.02 g/mol; m.p.: 80 – 82°C; 1H NMR (400 MHz, $CDCl_3$): δ = 8.05 (s_{br}, 4H, perylene protons), 7.72 (s_{br}, 4H, perylene protons), 7.31 (s_{br}, 2H, NH) 7.13 (s, 4H, Ph-*H*), 6.92 (s, 2H, Ph-*H*), 5.69 (q, 3J = 6.9 Hz, 2H, CH), 5.02 (dd, 3J = 7.1 Hz, 2J = 14.3 Hz, 2H, CH₂), 4.33 (dd, 3J = 3.8 Hz, 2J = 14.3 Hz, 2H, CH₂), 2.59 (m, 8H, CH₂), 1.69 (d, 3J = 6.7 Hz, 6H, CH₃), 1.58 (m, 8H, CH₂), 1.33-1.12 (m, 72H, CH₂), 0.85 (t, 3J = 7.0 Hz, 12H, CH₃); HRMS (ESI pos.; acetonitrile/ $CHCl_3$), calculated for ($[M+Na]^+$): 1408.9727, found m/z = 1408.9761; elemental analysis calculated (%) for $C_{92}H_{128}N_4O_6$: C 79.72, H 9.31, N 4.04; found: C 79.40, H 9.31, N 3.97; $\lambda_{max}(CHCl_3)$ / nm 528, 491 and 460 ($\epsilon / M^{-1}cm^{-1}$ 86900, 52400 and 19300).

3. ^1H NMR and mass spectra of PBI 2

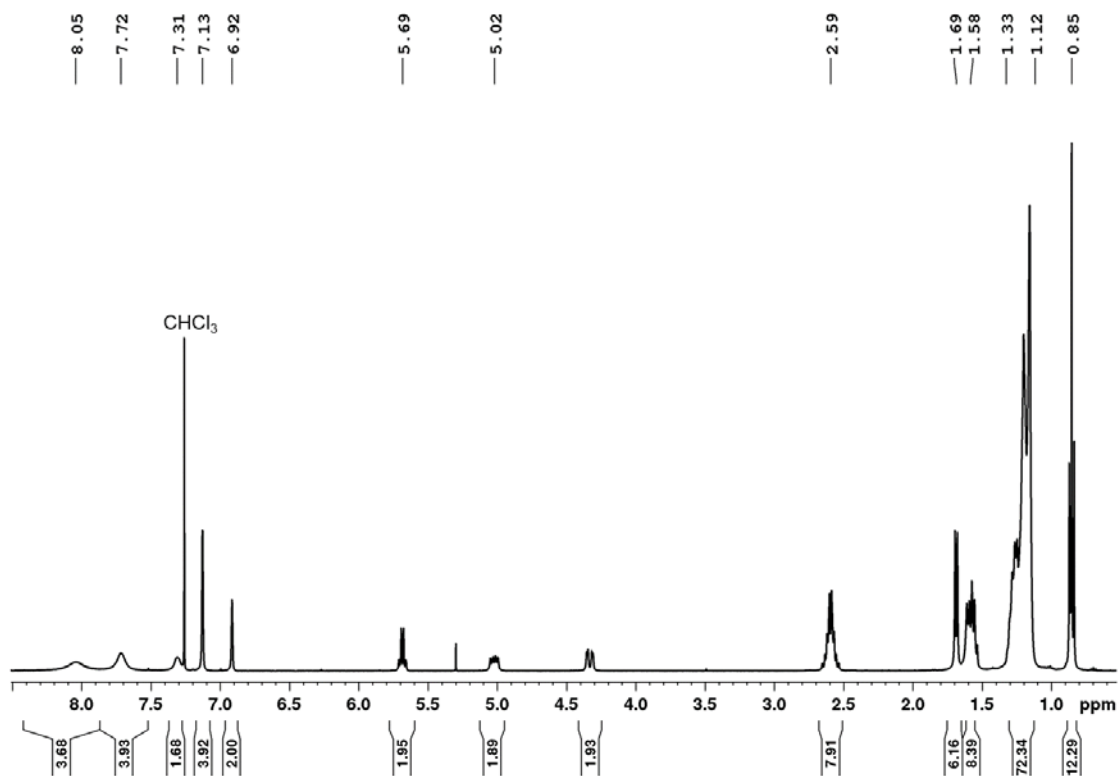


Fig. S1: ^1H NMR (400 MHz) spectrum of PBI 2 in CDCl_3 at 295 K.

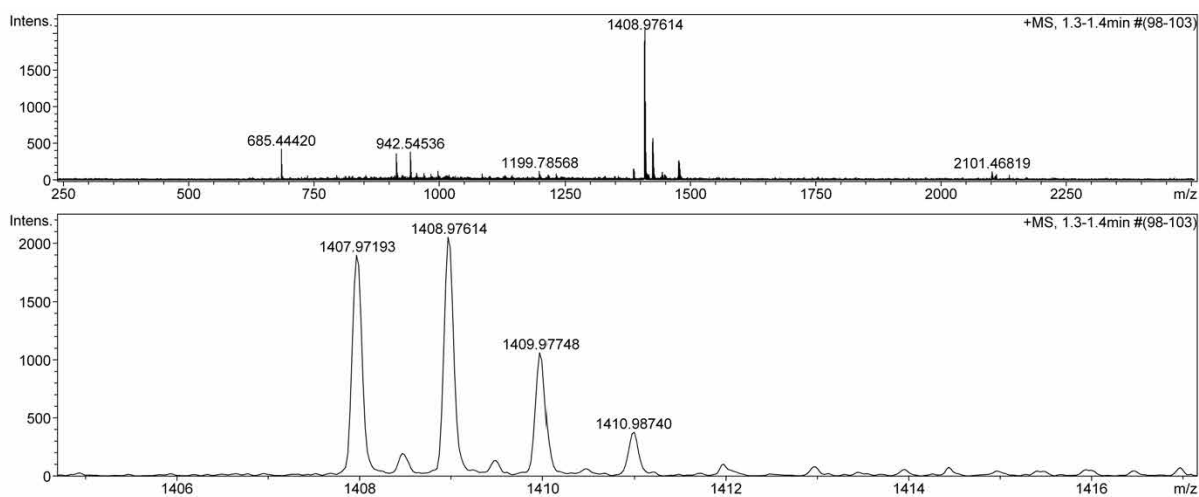


Fig. S2: HRMS-ESI (pos. mode; acetonitrile/ CHCl_3) spectrum of PBI 2.

4. Aggregation of PBI 2

In the polar solvent chloroform only the initial dimerization can be observed with a dimerization constant of $K_2 = 1.3 \cdot 10^3 \text{ M}^{-1}$ (Figure S3).

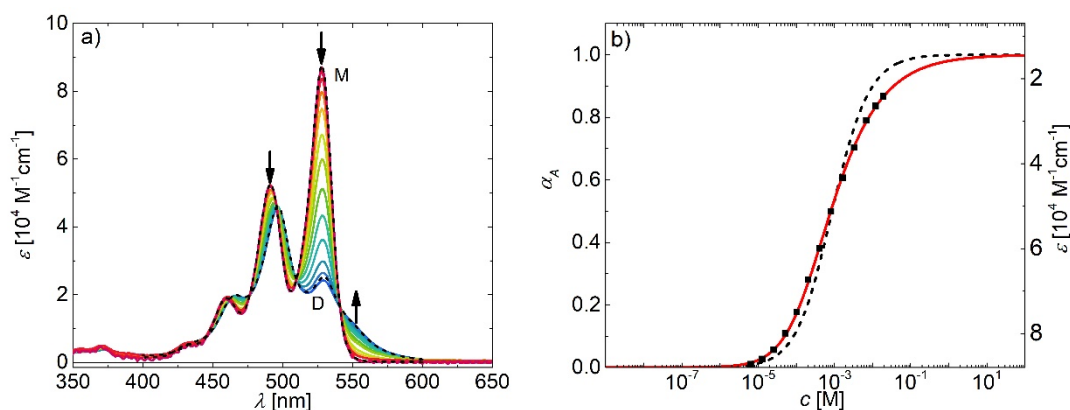


Fig. S3: a) Concentration-dependent UV/Vis absorption spectra of PBI 2 in CHCl_3 ($c = 6.4 \times 10^{-6} - 1.2 \times 10^{-2} \text{ M}$) at 293 K. The dotted lines are the calculated monomer (M) and dimer (D) spectra from available data based on the dimer model. Arrows indicate the spectral changes upon increasing concentration. b) Analysis of the concentration-dependent data at 528 nm according to the dimer (red line) and isodesmic (black dashed line) aggregation models ($R^2 = 0.999$ for dimer fit). Left and right axes display the degree of aggregation and extinction, respectively, for a direct comparison.

The aggregation behavior of PBI 2 was analyzed by means of the recently published anti-cooperative aggregation model^[S3] with a global analysis of the concentration-dependent extinction spectra in toluene, see Fig. S4a. The aggregation constants for dimerization was determined by this analysis to $K_2 = 9.0 \cdot 10^3 \text{ M}^{-1}$ and for further elongation $K = 540 \text{ M}^{-1}$. Fit and experimental data nicely coincide, as demonstrated for some characteristic wavelength in Fig. S4b.

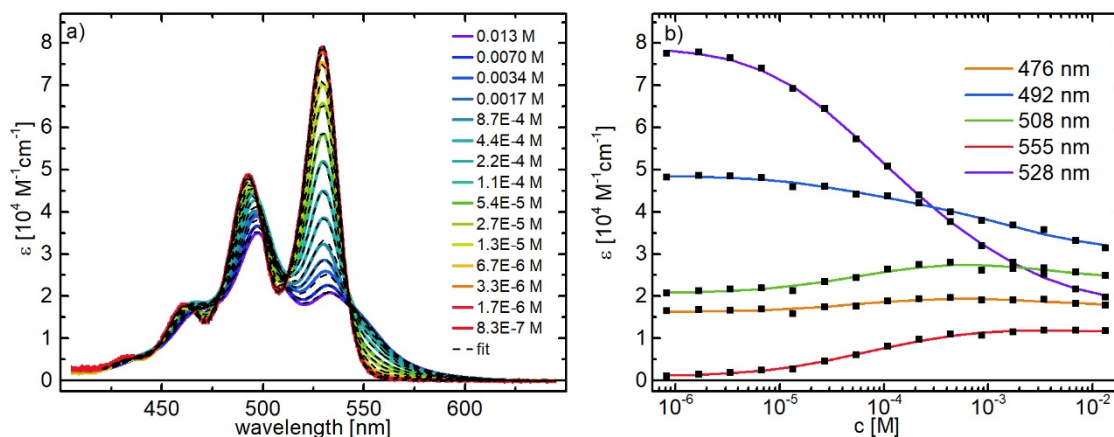


Fig. S4: a) Concentration-dependent apparent extinction coefficient of PBI **2** in toluene at 295K (colored curves) and global analysis with the K_2 - K model for anti-cooperative growth (black dashed curves). b) Fit of the K_2 - K model for anti-cooperative growth (colored lines) to the concentration-dependent apparent extinction coefficient (squares) at various wavelength.

To confirm the results obtained by UV/Vis absorption spectroscopy, ^1H and DOSY NMR studies for PBI **2** were performed in CDCl_3 . The concentration-dependent ^1H NMR spectra of PBI **2** were recorded in the concentration range of $5.2 \cdot 10^{-6} \text{ M}$ to $1.1 \cdot 10^{-2} \text{ M}$ (Fig. S5a,c).

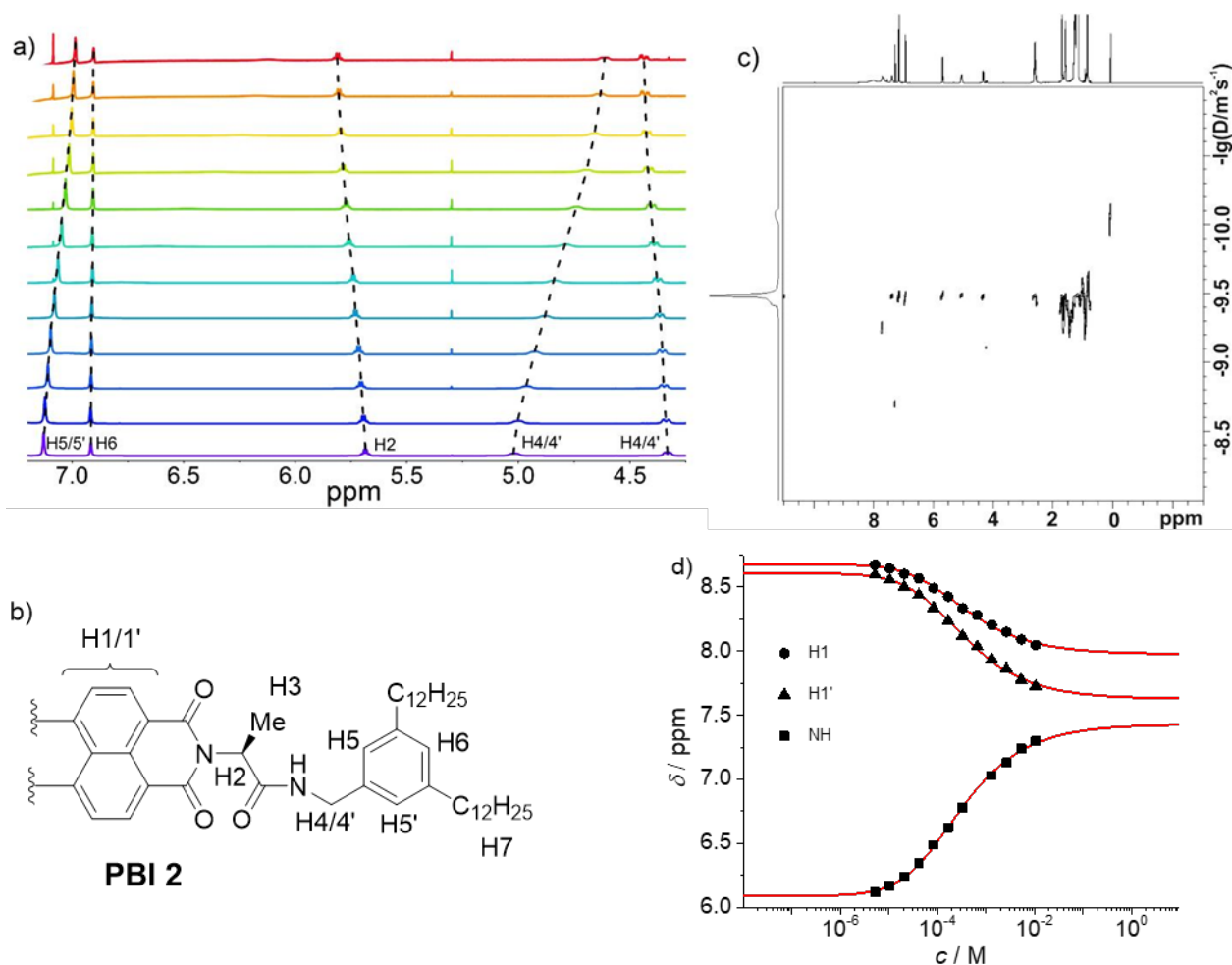


Fig. S5: a) Changes of the chemical shifts of PBI **2** protons (H2, H4/4', H5/5' and H6) in concentration-dependent ^1H NMR spectra (600 MHz) in CDCl_3 at 298 K ($1.1 \times 10^{-2}\text{ M}$ – $5.2 \times 10^{-6}\text{ M}$). b) Structure of one half of the symmetric PBI **2** with numbering of significant protons. c) DOSY NMR (600 MHz) spectrum of PBI **2** at $c = 2.0 \times 10^{-2}\text{ M}$ in CDCl_3 at 293K. The diffusion coefficients D [$\text{m}^2\text{ s}^{-1}$] are plotted in a logarithmic scale against the chemical shift δ [ppm]. d) Fitting of the concentration-dependent chemical shift (δ) changes of protons H1 and NH to the dimer model by means of nonlinear least-squares analysis as representative examples (correlation coefficient $R^2 = 0.999$).

With increasing concentration, the signals of the perylene protons (H1/1') show a considerable upfield shift from 8.7 and 8.6 ppm to 8.1 and 7.7 ppm, respectively, indicating π - π -interactions between the PBI molecules (black symbols in Fig. 5d).^[S4] On the other hand, the signal of the amide NH proton is displaced to the downfield, from 6.1 to 7.3 ppm, implying the formation of hydrogen bonds (black symbols in Fig. S5d).^[S5] Other protons of PBI **2** exhibit only small changes ($\Delta\delta < 0.4$ ppm, see Fig. S3a). The downfield shift of H5/5' upon increasing concentration is referred to the weak C-H \cdots O hydrogen bonding to the carbonyl oxygen atom. The similar upfield shift of H2 and H6 protons can be attributed to the aromatic shielding effect

by the neighboring PBI dye upon π - π -stacking. The two signals for diastereotopic protons H4 and H4' of PBI **2** are strongly separated at higher concentrations.

The concentration dependent changes of the proton signals could nicely be fitted with the monomer-dimer model, which corroborates the results of UV/Vis spectroscopic studies as illustrated in Fig. S5d for the perylene protons H1/1' and the amide NH proton. The fitting of the chemical shift changes of the protons of PBI **2** indicated in the structure (Fig. S3b) afforded an average dimerization constant K_2 of $3 * 10^3 \text{ M}^{-1}$ and the degree of aggregation α_A between 1 % and 90 % (Table S1).

Table S1: Dimerization constants (K_2) and degrees of aggregation (α_A) obtained in the considered concentration range ($5.2 * 10^{-6} - 1.1 * 10^{-2} \text{ M}$) from the best fitting of the chemical shift changes of the protons of PBI **2** in CDCl_3 .

Protons	H1	H1'	NH	H2	H3	H4	H4'	H5/5'
$K_2 / 10^3 \text{ M}^{-1}$	2.7 ± 0.1	2.9 ± 0.1	3.4 ± 0.1	2.9 ± 0.1	3.5 ± 0.1	3.1 ± 0.1	3.5 ± 0.1	2.9 ± 0.1
α_A^a	1 – 90 %	1 – 90 %	2 – 90 %	1 – 90 %	2 – 92 %	1 – 90 %	2 – 92 %	1 – 89 %

^a α_A value at the lowest concentration of $5.2 * 10^{-6} \text{ M}$ and the highest concentration of $1.1 * 10^{-2} \text{ M}$, respectively.

These values are in the same range as those obtained from UV/Vis absorption studies. Thus, both spectroscopic methods provide congruent results on the aggregation process of PBI **2**.

5. Determination of the fluorescence quantum yields of PBI 1 and PBI 2 monomers

The monomer fluorescence quantum yields Φ_M of PBI 1 and PBI 2 were determined for highly diluted solutions in toluene in 10 mm cuvettes. The concentration of PBI 1 was $4 \cdot 10^{-7}$ M and that of PBI 2 was $6.5 \cdot 10^{-7}$ M. At this concentration, more than 96 % of PBI 1 and more than 99 % of PBI 2 prevail in their monomeric state according to our aggregation studies described before and reported previously^[S3]. An emission contribution from aggregates in the case of PBI 1 was ruled out by a scan of the excitation wavelength in the interval from 450nm to 500 nm with a step size of 5 nm, see Fig. S6. The normalized emission excited with different

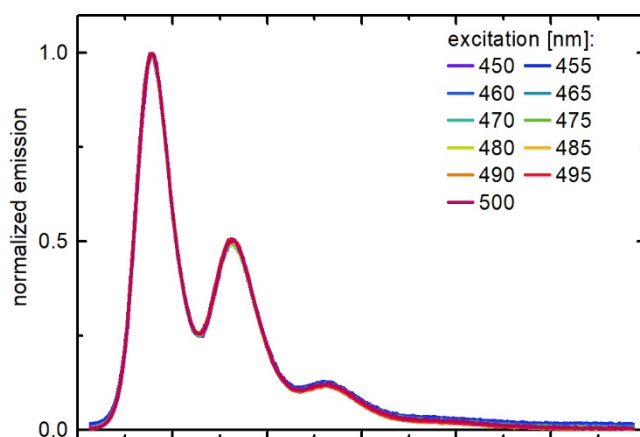


Fig S6: Normalized emission of PBI 1 in toluene with a concentration of $4 \cdot 10^{-7}$ M excited with different excitation wavelength.

wavelength show no shape variation, such that we conclude that the small amount of 4 % dimers in the case of PBI 1 is below the detection limit. The reference compound was PBI-ref2 in toluene with a Φ of 100 %. The polarization between excitation and emission was set to magic angle and the emission detection was in perpendicular direction with respect to the excitation. The resulting monomer quantum yield of PBI 1 is 27 % and that of PBI 2 is 100 %.

6. Calibration of monochromators

The three involved monochromators (excitation and emission monochromators of the emission spectrometer as well as the monochromator of the absorption spectrometer) were calibrated respectively checked as suggested by the suppliers. As the use of the species averaged

method and the site selective method to determine the Φ_A do not always allow to excite at a desirable extrema position of the absorption band, a uniform calibration of excitation monochromator (emission spectrometer) and absorption monochromator (absorption spectrometer) is necessary. To this end a self-consistent check and a comparison between these two monochromators is necessary. For this purpose we have developed a special routine to satisfy an accurate calibration. Starting with calibrated monochromators the routine is the following:

1. Measure the absorption of a sample with the absorption spectrometer.
2. Measure the absorption of the same sample with the emission spectrometer. This is done by adding a halogen lamp as additional light source to the sample chamber of the emission spectrometer in line with the detection monochromator such that the lamp can be used to measure the absorption of a sample with the emission monochromator. Then the lamp is shined through a reference sample (cuvette with solvent) and the spectra of the halogen lamp is measured (T_0). Subsequently, the reference sample is replaced by the sample and the lamp spectra is measured once more (T). The optical density (OD) of the sample is then calculated according to:

$$OD = -\log T / T_0.$$

A small baseline correction was necessary as a reproducible measurement is difficult in this way.

3. Both absorption measurements are compared, the one done with the absorption spectrometer and the one measured with the emission monochromator of the emission spectrometer. The comparison is displayed in Fig. S7. As these two measurements of the OD of the same sample nicely coincide we are able to demonstrate a uniform calibration of the monochromator in the absorption spectrometer and the emission monochromator in the emission spectrometer.

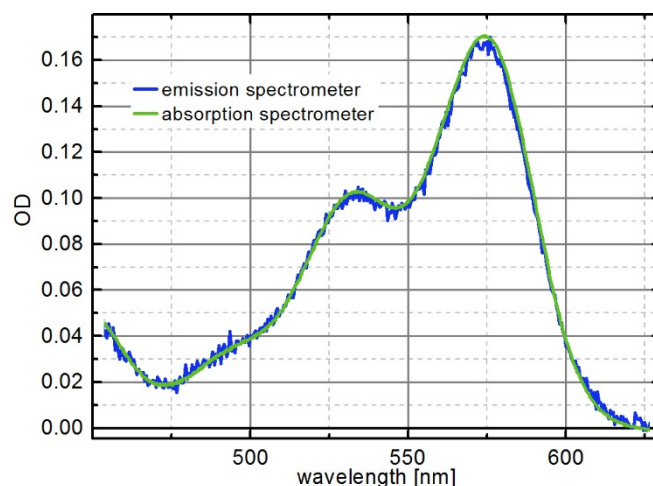


Fig. S7: Measurement of optical density of test sample performed with the absorption spectrometer (green) and the emission spectrometer (blue). Details on measuring the absorption of a sample with the emission spectrometer are given in the text.

4. For the given spectrometer the calibration possibilities of the excitation monochromator of the emission spectrometer are very limited and only a poor calibration to first order was possible. Therefore, we used the well calibrated emission monochromator of the emission spectrometer to correct the excitation wavelength accordingly. To this end, the spectra of the excitation light was measured with the emission spectrometer by inserting a scattering sample in the sample chamber. The emission monochromator was protected with an $OD = 2$ filter before the entering slit. The measured spectra are displayed in Fig. S8. We see that the actual excitation wavelength deviates from the wavelength applied to the excitation monochromator. Since a better calibration could not be reached, we accepted it and corrected it in the following. To this end, we fitted Gaussians to the excitation spectra and used the center wavelength as excitation wavelength (λ_{excit}). Instead of 450 nm, 455 nm, 460 nm, 465 nm, 470 nm, 475 nm, 480 nm, 485 nm, 490 nm, 495 nm and 500 nm, which were the applied wavelength to the excitation monochromator, we used 451.2 nm, 456.0 nm, 460.7 nm, 465.4 nm, 470.2 nm, 475.2 nm, 480.5 nm, 485.7 nm, 491.0 nm, 496.2 nm, 501.3 nm to determine the optical density at the excitation wavelength.

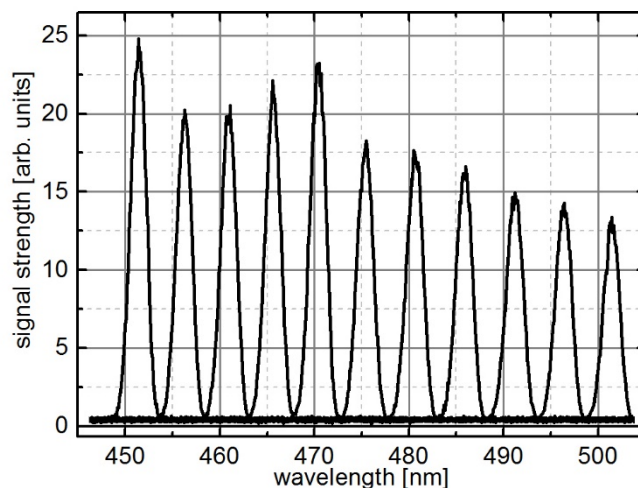


Fig. S8: Spectra of the excitation light measured with the emission monochromator of the emission spectrometer. Wavelength of 450 to 500 nm in steps of 5 nm were applied at the excitation monochromator.

7. Conditions for self-absorption free emission of PBIs

Self-absorption (SA) manifests as a red shift and decrease in emission strength in the high energy wing of the emission. The way to exclude self-absorption (SA) is to decrease the optical density of the sample and measure the emission. As soon as an optical density is reached where the blue wing and the peak position of the measured emission does not change any more, one can be sure to have SA free measurement conditions. Such a measurement was performed for the compound **PBI-ref 1** in toluene (Fig. S9).

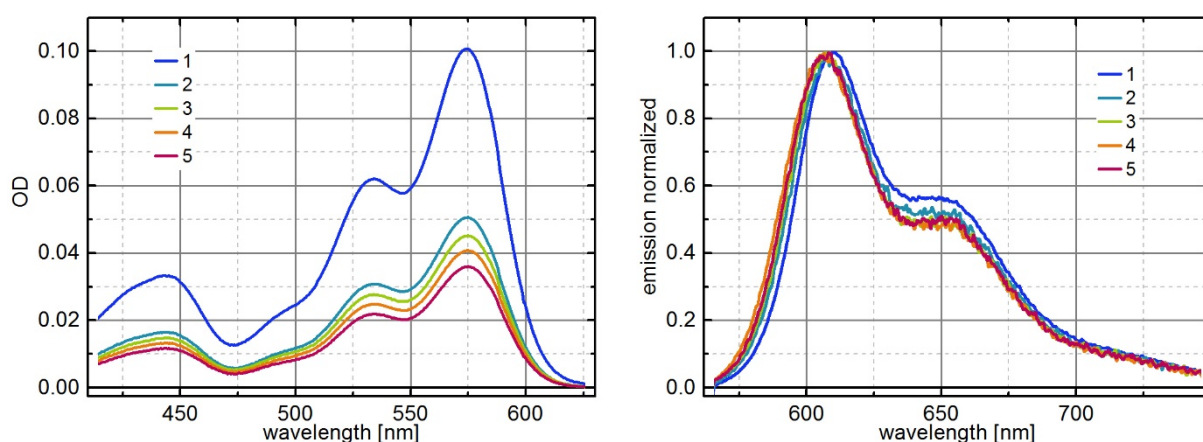


Fig. S9: Conditions for self-absorption. Absorption (left) and normalized emission (right) of five samples of **PBI-ref1** in toluene with different optical densities at the maximum of 0.1 (1, blue), 0.05 (2, cyan), 0.045 (3, green), 0.041 (4, orange) and 0.035 (5, red). The measurement setup was identical for all measurements performed in this paper.

Signatures of self-absorption, i.e. a red shift with increased contribution of the 0,1 vibronic shoulder at 650 nm as well as a reduced emission in the blue wing, are clearly visible for the highest optical density of 0.1. In the case of sample with optical density (OD) of 0.05 a weak red shift in the emission maxima is still present, whereas for the three lower optical densities no shape changes are present. Therefore, we conclude that self-absorption free emission is possible in the used measurement geometry for an optical density below 0.045 in the maximum.

Self-absorption free emission for our measurements is also supported by the low probability of reabsorption as it can be calculated in the following equation. The probability for self-absorption a depends on the spectral overlap of the absorption with the emission spectra:^[S6]

$$a = \int_0^{\infty} F(\lambda) \left(1 - 10^{-OD(\lambda)}\right) d\lambda$$

where the emission spectra $F(\lambda)$ is normalized to one $\int_0^{\infty} F(\lambda) d\lambda = 1$, and free of self-absorption according to the test displayed in Fig. S9. In all measurements performed in this paper the probability of self-absorption was kept below 1 %.

8. Excitation wavelength dependent emission of fluorescence standard PBI-ref 2 and PBI 2 in toluene

In the case that the fluorescence standard PBI-ref 2 is excited at different excitation wavelengths, the shape of the normalized emission is identical (Fig. S7), clearly revealing that only one species, the monomer, is present in solution. In contrast, the shape of the PBI 2 emission depend on the relative portion of excited monomer versus aggregate, which is wavelength dependent.

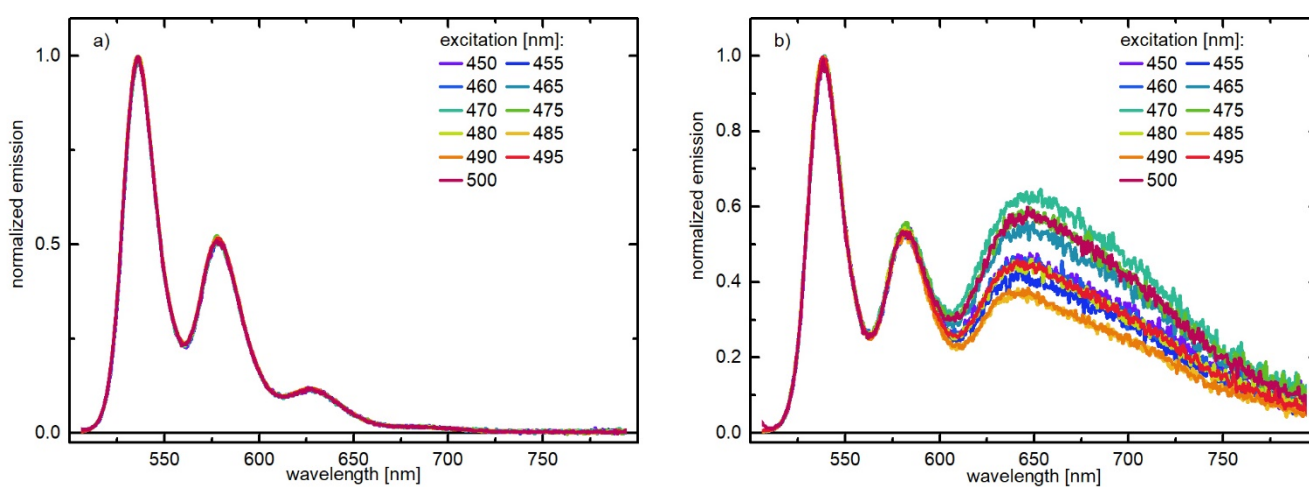


Fig. S10: Normalized emission of PBI-ref 2 (a) and of PBI 2 (b) in toluene for different excitation wavelengths. In case of PBI-ref 2 all spectra well coincide, whereas the relative portion of aggregate emission changes for PBI 2.

9. Scan of excitation wavelength for species averaged method PBI 2

The ratio of photons absorbed by monomers (X_M) are depicted on the left axis of Fig. S11. The amount of excited monomers is dependent on the degree of aggregation α_A and the ratio between monomer extinction and aggregate extinction at the respective excitation wavelength. The right axis is the measured Φ_A of the aggregate at the respective excitation wavelength. The black line is the mean value and the dashed lines are the standard deviation.

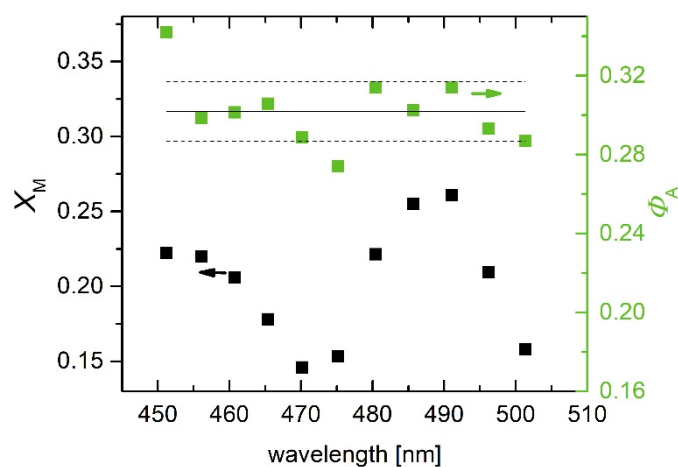


Fig. S11: Determination of aggregate fluorescence quantum yield of PBI 2 in toluene ($8.0 \cdot 10^{-4}$ M) with the species averaged method (green) and the resulting ratio of excited monomers X_M (black) at different excitation wavelengths.

10. Determination of ratio of excited monomers from the aggregation study

Our UV/Vis aggregation studies allow to calculate the fraction of each of the species in dependency of the total molecular concentration, see Fig. 7 in the main article. From this data we can take the fraction of each species at the desired concentration of 8.0×10^{-4} M. We find a relative content of monomers of 0.20, dimers of 0.55 and oligomers of 0.25 for PBI 2. Please note that these values are the percentage of PBI 2 molecules in the respective state of aggregation. The molar extinction coefficients of the respective species at the excitation wavelength of 465 nm can be taken from Fig. 1a in the main article and are $\epsilon_M = 16545 \text{ M}^{-1} \text{ cm}^{-1}$ (monomer), $\epsilon_D = 19775 \text{ M}^{-1} \text{ cm}^{-1}$ (dimer), $\epsilon_O = 15745 \text{ M}^{-1} \text{ cm}^{-1}$ (oligomer). With this numbers we can calculate ratio of photons that were absorbed by monomers:

$$X_M = \frac{0.20 * 16545}{0.20 * 16545 + 0.55 * 19775 + 0.25 * 15745} = 0.1826 \approx 18 \%$$

11. Determination of aggregate quantum yield of PBI1 with species averaged method

The species averaged method to determine the fluorescence quantum yield of the PBI 1 aggregate was carried out with a PBI 1 concentration of $8.7 \cdot 10^{-4}$ M in toluene in 10 μm cuvettes. The fluorescence standard was PBI-ref2 with a concentration of $5.4 \cdot 10^{-4}$ M in toluene. Both samples were excited in the interval from 450 nm to 500 nm in step size of 10 nm. The obtained values for Φ_A and for X_M are displayed in Fig. S12

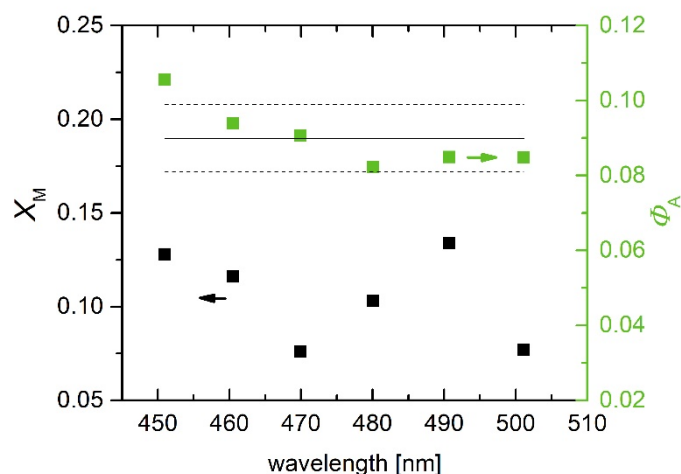


Fig. S12: Determination of aggregate fluorescence quantum yield of PBI 1 in toluene ($5.4 \cdot 10^{-4}$ M) with the species averaged method (green) and the resulting ratio of excited monomers X_M (black) at different excitation wavelengths

The mean value of Φ_A for the different excitation wavelength is 9.0 % and the standard deviation is 0.9%.

12. Histogram of aggregate size for characteristic concentrations

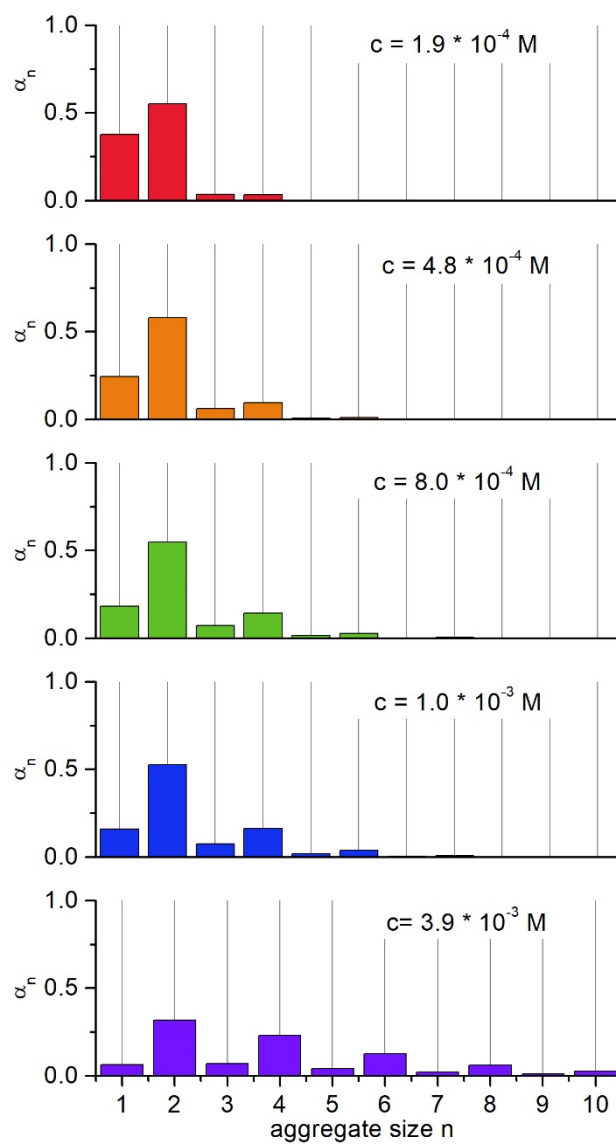


Fig. S13: Histograms obtained from the aggregation study for PBI 2 in toluene for the five concentrations used to determine Φ_A .

13. Error discussion

The experimental errors for conventional Φ measurements are in general given between 5 % and 10 % and include emission corrections and the reliability of the standard.^[S7] In the present case, additional errors such as the low optical densities required to prevent SA in the front face geometry and experimental errors that come along with the determination of X_A in case of the species averaged method add on top, thus we expect higher experimental errors.

The mean value is calculated as:

$$\Phi_{A,\text{mean}} = \frac{1}{N} \sum_{i=1}^N \Phi_{A_i} = 28.2 \%$$

where Φ_{A_i} are the five measurement values given in Table 1 in the main paper. The standard error of the mean is:

$$\sigma_{\text{mean}} = \sqrt{\frac{\sum_{i=1}^N (\Phi_{A,\text{mean}} - \Phi_{A_i})^2}{N(N-1)}} = 1.28$$

In order to reach a confidential interval of 95 %, σ_{mean} has to be multiplied with 2.776 for four degrees of freedom (t-distribution tables). Therefore, the complete result reads:

$$\Phi_A = 28 \% \pm 4 \% = 28 \%(1 \pm 0.14)$$

14. References

- S1 D. D. Perrin, W. L. F. Armarego and D. R. Perrin. *Purification of laboratory chemicals*; Pergamon Press, Oxford: New York, 1980.
- S2 Y. Xu, S. Leng, C. Xue, R. Sun, J. Pan, J. Ford and S. Jin, *Angew. Chem. Int. Ed.* 2007, **46(21)**, 3896–3899.
- S3 J. Gershberg, F. Fennel, T. H. Rehm, S. Lochbrunner and F. Würthner, *Chem. Sci.* 2016, **7(3)**, 1729–1737.
- S4 a) C. Shao, M. Grüne, M. Stolte and F. Würthner; *Chem. Eur. J.* 2012, **18**, 13665-13677; b) J. S. Wu, A. Fechtenkötter, J. Gauss, M. D. Watson, M. Kastler, C. Fechtenkötter, M. Wagner and K. Müllen, *J. Am. Chem. Soc.* 2004, **126**, 11311-11321; c) D. H. Zhao and J. S. Moore, *J. Org. Chem.* 2002, **67**, 3548-3554.
- S5 a) F. H. Beijer, H. Kooijman, A. L. Spek, R. P. Sijbesma and E. W. Meijer, *Angew. Chem. Int. Ed.* 1998, **37(1-2)**, 75–78; b) C. Rether, E. Verheggen and C. Schmuck; *Chem. Commun.* 2011, **47(32)**, 9078–9079; c) R. Wyler, J. de Mendoza and J. Rebek, *Angew. Chem. Int. Ed.* 1993, **32(12)**, 1699–1701.
- S6 a) M. Lagorio, L. Dicelio, M. Litter and E. Roman, *J. Chem. Soc., Faraday Trans.* 1998, **94(3)**, 419–425; b) P. J. Hammond, *Chem. Phys.* 1979, **70(8)**, 3884–3894.
- S7 C. Würth, M. Grabolle, J. Pauli, M. Spieles and U. Resch-Genger, *Nature Prot.* 2013, **8(8)**, 1535–1550.